ON THE EVOLUTION-DYNAMICS OF TROPICAL OCEAN-ATMOSPHERE ANNUAL-CYCLE VARIABILITY

Sumant Nigam
Department of Meteorology
University of Maryland, College Park, MD 20742-2425

and

Yi Chao
Earth and Space Sciences Division, J.P.L.
California Institute of Technology, Pasadena, CA 91109-8099

(submitted to the *J. Climate* on October 17, 1994)

Abstract

The structure of ocean-atmosphere annual-cycle variability across the global tropics is extracted from the Comprehensive Ocean-Atmosphere Data Set (COADS) surface winds and SSTS, and oceanic heat-content simulation from a nonlinear shallow water model (forced by COADS wind stress) using the co-variance based rotated principal component analysis technique.

'l'he coupled annual-cycle variability is compactly describable using *two* modes that are in temporal quadrature, and whose structures are insensitive to the inclusion/exclusion of oceanic heat-content in the combined variability analysis. The *first* mode, peaking in July (and January), represents large-scale monsoonal flow onto the warmer continents: Indo-China, Central America, and western Africa, The second annual-cycle mode peaks in October (and April) when it represents the extreme phases of SST annual variability in the eastern oceans.

An analysis of the associated surface-momentum balance shows the equatorial flow in the cold-tongue's core region to be dynamically consistent with the 'SST-gradient driven' sea-level pressure gradients, and more so, when the impact of near-surface static-stability variation on horizontal-momentum dissipation is factored in. inspection of temporal phasing of the extracted annual-cycle related zonal and meridional winds w.r.t. SSTS furthermore shows easterly-tendency to lead local cooling in the off-coastal longitudes (westward of 100°W) by about a month.

Taken together, this indicates that the cold-tongue's westward expansion in the off-coastal eastern Pacific and Atlantic results from the *local* interaction of zonal wind and zonal SST-gradient, particularly, at the tongue's leading edge; the westward expansion of warm-phase SSTS proceeds similarly. A 'westward expansion hypothesis' encapsulating these coupled interactions is proposed.

The weak SST annual-cycle in the off-coastal northern equatorial Indian Ocean, on the other hand, appears to be driven by modulations of latent-heat flux and oceanic mixed-layer stirring that are induced by robust surface wind-speed variability associated with the Asian monsoon,

J. Introduction

The ocean-atmosphere seasonal cycle in the eastern Pacific and Atlantic is notable for its robustness, and distinctiveness from the seasonal march at other tropical longitudes. The coupled seasonal cycle is also remarkable because its period is twice that of the dominant external forcing in these latitudes, While a comprehensive documentation of seasonal-cycle variability in the tropical Pacific has existed since Horel's (1982) annual-harmonic analysis of several related oceanic and atmospheric variables, the interest in understanding the dynamics of the coupled ocean-atmosphere seasonal-cycle evolution is rather recent (e.g., Chao, 1990), and, principally, spurred by the need to better understand, model and predict the low-frequency El Niño Southern Oscillation (ENSO) variability. The latter is connected to aspects of seasonal-cycle variability in the eastern Pacific (Rasmussen and Carpenter, 1982), and known for its global climatic impacts (Ropelewski and Halpert, 1987).

The mechanism(s) responsible for the unique seasonal evolution of the tropical ocean-atmosphere system have been explored by Mitchell and Wallace (1992) and Wang (1992), and from a dynamical instability perspective by Chang and Philander (1 994), Mitchell and Wallace's (1992) diagnostic analysis reveals the importance of interactions/feedbacks of the eastern ocean basins with the adjoining land-masses, and with insolation via shortwave modulation by the low-level stratus decks, Mitchell and Wallace (1 992) argue for a leading role of the *meridional* windstress changes at the northern edge of the equatorial waveguide (that are driven by the evolving Central American monsoons) in promoting the westward expansion of the SST cold-tongue via an oceanic mixed-layer remote response.

Wang's (1992) multiv variate extended empirical orthogonal function analysis of outgoing longwave radiation and Comprehensive Ocean-Atmosphere Data Set's (COADS) surface winds,

sea-level pressure and SSTS yields two annual-cycle related modes: the anti-symmetric (about the equator) monsoonal mode and the quasi-symmetric equatorial mode. The latter captures the extreme phases of SST variability in the equatorial eastern Pacific. Wang's analysis indicates that the SST cold-tongue evolution results from a complex interaction of these two modes, and that the northward shift of the ITCZ over the eastern Pacific in May is not controlled by the onset of the Central American monsoons,

Chang and Philander (1994) seek an explanation for the unique annual-cycle evolution in the eastern ocean basins via normal mode instability analysis of the annual-mean tropical ocean-atmosphere state. Their analysis yields a set of unstable coupled modes, the most unstable of which has infinite period, and a zonally symmetric but meridionally anti-symmetric SST structure about the equator (akin to Wang's monsoonal mode). Their study suggests that the coupled annual-cycle evolution in the eastern ocean basins is initiated by the monsoonal mode, but that the westward propagation of equatorial zonal winds and SST-- a notable feature of the coupled annual cycle, is due to another unstable coupled mode that has symmetric SS"1' structure and an annual period (akin to Wang's quasi-symmetric equatorial mode), Chang and Philander's (1994) analysis shows the annual-cycle variability to be unconnected with thermocline-depth variations, but is not quite revealing of the coupled dynamics encapsulated in their second annual-cycle related unstable mode.

It thus appears that there does not exist at the present time a succinct elucidation of the dynamics/thermodynamics governing the most fundamental aspect of coupled seasonal-climate evolution in the deep-tropics-- the westward and northward expansion of the Pacific cold-tongue during June-October, the primarily westward expansion of the Atlantic cold-tongue during May-September, and the eastward and northward expansion of the comparative] y weaker cold-

phase SSTS in the Indian Ocean during June–October.

The objective of this study is to contribute towards such an elucidation. It begins with the extraction of the coupled ocean-atmosphere annual-cycle variability structure from COADS surface winds and SS"1's, and oceanic heat-content simulation from a nonlinear shallow water model (forced by COADS wind stress) using the rotated principal component analysis (RPCA) technique, The COADS winds and SS"1' dataset is described in section 2, and the shallow-water model used in generating the concurrent ocean heat-content anomalies in section 3. The covariance-based RPCA technique of analyzing *combined* variability is briefly discussed in section 4, while a compact description of the tropical ocean-atmosphere annual-cycle in terms of the two-leading recurrent modes of combined variability is presented in section 5.

The dynamical diagnoses part is structured around the analysis of zonal and meridional surface-momentum balance in the core of the SST cold-tongue in sections 6A and B, and an examination of the role of zonal and meridional winds in promoting the westward expansion of the SST cold-tongue in section 6C. Momentum-balance and evolutionary-role assessments lead to the formulation of a 'westward expansion hypothesis' in section 6D. The robustness of the observational bases of the proposed 'westward expansion hypothesis' is ascertained in 6E, while subsection F concludes section 6 with the display and discussion of semi-annual variability in the eastern Pacific. The coupled seasonal-cycle evolution in the eastern Atlantic is compared with that in the eastern Pacific in section 7, and the salient features of seasonal-cycle evolution in the Indian Ocean basin are noted in section 8. Discussion and conclusions follow in section 9.

2. Datasets

The gridded COADS dataset used in this study was obtained from the National Meteorological Center's Climate Analysis Center (NMC/CAC). The COADS monthly-mean

surface winds from January 1950 to December 1987 were interpolated from a 2°x20 grid onto a 10x20 latitude-longitude grid between 30°S and 30°N to generate surface wind stress* that were, in turn, used to force a nonlinear shallow-water ocean model to simulate oceanic heat-content (: thermocline depth or upper-layer thickness). Anomaly-matrix size consideration in the undertaken combined variability analysis necessitated interpolation of the monthly-mean 2°x20 COADS SSTs and surface winds and the 10x20 simulated oceanic heat-content onto a 2°x60 latitude-longitude grid, The anomalies were then converted into *two*-month averages to avoid potential aliasing of tropical intraseasonal variability into longer-period variability. The analysis was restricted to oceanic regions through the use of a land-sea mask containing 1399 oceanic grid points at 2°x60 latitude-longitude resolution; even at this coarse spatial-temporal resolution, the combined anomaly matrix size was 5596 x 228.

3. Shallow-water model

The oceanic heat-content is generated from a nonlinear absolute potential enstrophy conserving shallow-water model (Sadourney, 1975; Philander and Pacanowski, 1981a). The model depth is 281 m and the reduced gravity is 3.2 $cm\,s^{-2}$. This corresponds to the first baroclinic mode that is primarily responsible for the adjustment of the upper ocean. A Laplacian friction is used with a coefficient of $5 \times 10^{7} cm^{2} s^{-1}$. The shallow water model is solved on a 10x20 latitude-longitude spherical grid between 30°S and 30°N using realistic coastal geometry. The horizontal velocities are assumed to vanish at ±30°, which tantamounts to the placement of rigid walls with the no-slip condition at these latitudes.

'Surface wind stress was generated from surface winds using a drag coefficient $C_D = 1.6 \times 10^{3}$. As wind stress is a nonlinear function of surface winds, its estimation from n~onthly-mean surface winds is likely to be somewhat underestimated. Better estimates of windstress, devoid of this and other deficiencies, are now available from Da Silva et al.'s (1993) re-analysis of COADS observations.

The model was started from rest, and integrated for nine years while being forced by the COADS *climatological* monthly-mean wind stress field (that were linearly-interpolated to the integration calendar-day and time-step); after a spin-up phase, the simulated seasonal changes during the 7th, 8th and 9th year became rather similar, suggesting the establishment of a quasi-equilibrium response in the tropical Pacific. After this 9-year spin-up, the model was forced by COADS monthly-mean wind stress from 1950 to 1987. The variability of the shallow-water model simulated oceanic heat-content during 1967-1979 has been compared with tide-gauge measurements, and with the simulations of the GFDL's OGCM, and the agreement amongst them was good (Chao, 1990; Chao et al., 1993).

4. **Analysis method**

The rotated principal component analysis (RPCA) technique is employed to extract the recurrent modes of *combined* ocean-atmosphere annual-cycle (and interannual) variability across the global tropics. The RPCA technique can isolate recurrent modes of combined variability (of any number of variables) by simultaneously analyzing the structure of the auto-covariance matrices (associated with each variable) *and* the cross-covariance matrices (between all pairs of variables in the combination). The efficacy of this method in extracting the truly-coupled variability modes increases with the number of variables in the combination (Nigam and Shen, 1993); in case of a four-variable combination, like the *one* used in this study, the cross-covariance submatrices outnumber the auto-covariance ones by 3 to 2. When analyzing combined variability, the individual variables are put on par with each other by dividing each of them by the square-root of their spatially-averaged variance (and not by their local standard deviation). The advantages of this strategy and a detailed description of RPCA algorithm is given in section 2 and appendix A, respectively of Nigam and Shen (1993). The RPCA analysis

of combined variability of U_s, V_s, SSTS and oceanic heat-content[2] (H_{con}) undertaken here is based on the *spatial* recurrence criterion alone, but such analysis should nonetheless provide interesting *evolutionary* information if the spatial variability associated with different frequencies is sufficiently distinct, and when H_{con} variability is not in phase with that of the other 3 variables (as, for example, on the interannual time-scale).

The annual-cycle related variability has traditionally been extracted by focussing on the evolution of climatological month] y-means (e.g., Mitchell and Wallace, 1992) but the results obtained from such analysis can be potentially compromised by the presence of significant sub-annual harmonic variability (e.g., semi-annual variability in the tropics). Alternative strategies include performing harmonic analysis of local temporal variability (e.g., Here], 1982), an extended empirical orthogonal function (EEOF) analysis of spatio-temporal variability y (e. g., Weare and Nasstrom, 1982), or the nearly equivalent multi-channel singular spectrum analysis (M-SSA) of combined variability (e.g., Robertson et al., 1994). The undertaken analysis, in contrast, focuses on recurrent spatial structures of variability (both within a variable and across the variable-combination), and succeeds in extracting annual-cycle related variability only because of the latter's distinctive spatial structure. The extracted annual-cycle variability is represented by two modes that are in temporal quadrature with a spatially-dependent lead/lag relationship.

5. Compact description of tropical ocean-atmosphere annual-cycle variability

The two-leading recurrent modes of combined variability, shown in Figs.1 and 2, and explaining 41% and 19% of domain-averaged variance, respective] y, are clear] y associated with annual-cycle variability across the global tropics; the phase relationship between their coefficient

[2] H_{con} and SSTS arc somewhat directly related to each other in the eastern tropical-ocean basins where the thermocline is climatologically shallower; however, as such regions arc, areally, a modest fraction of the global tropics, wc assume H_{con} and SSTS to be quasi-independent variables in the undertaken analysis.

time series indicates that these two modes are temporally in quadrature. The structure of these annual-cycle modes is however insensitive to the inclusion/exclusion of H_{con} anomalies in the combined variability analysis[3], in accord with the findings of Chang and Philander (1994) and Wu (1994) regarding the unconnectedness of thermocline-depth variations and SST annual-cycle variability,

The first mode, peaking in July[4], is the 'monsoons] mode' as apparent from the robust large-scale onshore flow over the warmer northern continents: Indo-China, Central America, and western Africa. This mode has anti-symmetric (about the equator) zonal winds and quasi-symmetric meridional winds with a relative minimum in amplitude at the equator. The notable features of the SST component are its near anti-symmetricity about the equator, and the zonally-asymmctric structure in the equatorial central and eastern Pacific due to excursion of positive SST contours southward of the equator in the central Pacific[5], and nascent cold-tongue development about 2°S in the eastern Pacific (and Atlantic). In the eastern Pacific, this mode has considerable resemblance to Mitchell and Wallace's (1 992) climatological 'May minus March' differences in SSTS and surface winds, for the field-tendency [$=(3/\pi)$ times this difference] is in lag-quadrature with the field itself (as in any oscillation).

The second annual-cycle mode (Fig. 2) peaks in October, and is characterized also by anti-symmetric zonal winds, but weakly anti-symmetric meridional winds, particularly, in the

---

[3]When H_{con} is excluded from the combined variability y anal yses, the t we-leading annual -cycle modes explain 49% and 19% of the domain-averaged variance, respectively.

[4]Use of two-month averaged data for annual-cycle variability analysis affords a phase resolution of 60°, which is insufficient to accurately locate the phase maximum/minimum. The variability analysis was therefore repeated with monthly-averages, and that showed this mock to peak in July.

[5]This is a robust feature as it is present in the annual-cycle modes extracted from analyses of monthly-averages, two-month averages (both JF,MA,MJ, etc., and DJ,FM, AM, etc.), and three-mon[h averages.

central/eastern Pacific (and Atlantic) where the fully matured SST cold-tongue(s) are now quasi-symmetrically placed about 2°S, "l"his mode represents the peak phases of annual-cycle variability in the eastern ocean basins. Its structure shows the south central and eastern Pacific to be devoid of significant annual-cycle related surface-wind activity during the transitional seasons. The coefficient time series of the second mode, unlike that of the first mode, contains evidence of weak amplitude-modulation on the interannual time-scale---not surprising, in view of the linkage between El Niño evolution and the phase of seasonal-cycle variability in the *eastern* Pacific (Rasmussen and Carpenter, 1982),

The positive SSTS (with weak gradients) in the *equatorial* central Pacific (1 80°- 120°W) occurring westward of the nascent cold-tongue in July (in Fig. 1) appear to result from the persistence of warm-tongue SSTS from April when the 'monsoonal mode' has near-zero amplitude, and the second annual-cycle mode (Fig. 2) maximum negative amplitude. This aspect of SST annual-cycle variability is more clearly brought out in Fig. 3 which shows the composite seasonal-march of the '4 °S–EQ latitude-band averaged' SSTS in both of the annual-cycle variability modes. These modes are in temporal quadrature, as noted before, but their quadrature phase-relationship is spatially variable (lead/lag)----for example, the second combined-mode's SS"1's *lag* the first mode's SSTS by 3-months across the equator excepting the (1800-- 120°W) sector and the Maritime Continent longitudes (90°E– 120011), where the former *lead* the latter. Such spatial variability in the temporal quadrature phase-difference between two annual-cycle modes essentially depicts spatial variability of phase in harmonic analysis, e.g., the westward propagation of phase of the SST annual-harmonic in the equatorial eastern Pacific (Horel, 1982). The composite seasonal evolution of total SST annual-cycle variability (: RLV1+RLV2), shown in the bottom panel of Fig. 3, graphically displays this coherent westward phase-propagation in

the equatorial eastern Pacific and Atlantic basins, The westward propagation of SST-phase continues coherently past the dateline even though SST annual-cycle amplitudes are much smaller there. In contrast with the above, a 'somewhat less coherent' but eastward SS1'-phasc propagation is evident over the equatorial Indian ocean, with the SST annual-cycle signal emanating from the coastal upwelling/downwelling changes along the Somali coast.

6. Evolution of the Pacific SST cold-tongue

The growth of SS1 cold-tongue in the northern summer-to-autumn months is purportedly initiated by the May/June monsoonal winds that are predominantly along-shore (and northward) over the colder southern continent, and on-shore over the warmer Central American landmass (Mitchell and Wallace, 1992). 'l'he July southeast trades in the equatorial eastern Pacific comprise of northward cross-equatorial flow and equatorial easterlies that appear to bc dynamically consistent with the SST-gradient driven sea-level pressure (psi) gradients (Lindzen and Nigam, 1987), The longitudinal structure of the 4°S–EQ band-averaged July and October surface-winds, SSTS, and $(SST)_x$ is displayed in Fig. 4 to facilitate dynamical understanding of the forcing of *zonal* surface-winds in the cold-tongue's core-region- -for the influence of meridional SST-gradients will be minimal in cold-tongue longitudes in latitude-band averages that are centered on the SST cold-tongue's core latitude (-2°S).

A. The zonal momentum balance

We first focus on the forcing of the zonal wind component considering its potential role in promoting the cold-tongue's westward expansion via Ekman driven equatorial upwelling. The approximate momentum balance for steady tropical near-surface winds is: $\varepsilon_u u = fv - p_x/\rho_o$; $\varepsilon_v v = -fu - p_y/\rho_o$ where ε_u and ε_v are the Rayleigh friction coefficients with $\varepsilon_u < \varepsilon_v$ (Deser, 1993), and the rest of the notation standard. Clearly, the zonal variation of the Coriolis torque (fv), due

to *zonal variation* of the meridional wind[6], has the potential to obfuscate the recognition of any general phase relationship between the zonal wind and zonal SST-gradients in this 4°S-EQ band,

An inspection of the longitudinal structure of July SSTS and zonal winds in Fig. 4 shows the cold-tongue's western edge at -120"W (as determined from the zero-crossing of SSTs), but zonal SST-gradients to be maximum-negative further eastward (~95°W) just where the easterlies are the strongest. In the extreme eastern Pacific, the July zonal SST-gradient vanishes at 90°W, and is positive eastward of it; again, in accord with the Lindzen-Nigam hypothesis (hereafter, the I. N-hypothesis), the July zonal wind vanishes in the vicinity of 90"W, and is westerly further to the east. Westward of the cold-tongue's leading edge, the July zonal SST-gradients are weaker but still negative, and the zonal winds weak easterlies, as expected. The zonal SST-gradient vanishes at -1 50°W, and remains quite weak westward of this longitude as cold-tongue SSTS are confined to the east of -130°W in July. For the same reason, the meridional SST-gradients are more significant westward of the cold-tongue's longitudes (i. e., westward of 150°W in July; see the SST-panel in Fig. 1), as also evident from the increased strength of the July southerl y flow in these longitudes. The forcing of zonal winds westward of 150"W is discussed in footnote 6.

The October zonal winds and SSTs in the longitudinally expanded cold-tongue core region exhibi a zonal phase relationship similar to that seen in the July period, e.g., the October zonal winds vanish at ~95°W, precisely, where $(SST)_x$ vanishes, and are westerly eastward of this

---

[6]More precisely, $u = -[\varepsilon_v p_x + f p_y]/\{\rho_0(f^2+\varepsilon_u\varepsilon_v)\}$, and $v = [-\varepsilon_u p_y + f p_x]/\{\rho_0(f^2+\varepsilon_u\varepsilon_v)\}$. At the central latitudc of the cold-tongue (or in the 4°S-EQ latitude-band average), v should be small in the cold-tongue's longitudes for its *direct* forcing by meridional SST-gradicnts vanishes there, i.e., the meridional SST-gradient contribution to p_y vanishes there, and so p_y is expected to be small in such longitudes. p_x, on the other hand, is *not* small in the cold-tongue's longitudes, but it is multiplied by $f_{2°S}$, so v should be small in these longitudes, in both July and October, as ascertainable from Fig. 4. Westward of the cold-tongue's longitudes, the SST-gradient related p_x is small but not the related p,; in these longitudes, u is determined by the meridional SST-gradient related p_y, and also by zonal variations in the "free" (i.e., SST-gradient *un*related) component of the pressure field. The asymmetry in ε_u and ε_v further bolster these arguments.

longitude where $(SST)_x$ is positive. Westward of -1 OO"W, $(SST)_x$ is negative and so are the zonal winds. The July and October $(S\ ST)_x$ are, in fact, quite comparable in the 135°W–1 10"W sector, but the zonal winds begin to differ westward of 120°W, with the October winds becoming more easterly. At 130°W, the October easterlies are twice as strong[7], and also stronger than the October easterlies at 11 O"W where $(S\ ST)_x$ is about twice as large as that at 130°W.

This longitudinal discrepancy in October is, perhaps, a reflection of enhanced ε_u (and ε_v) across longitudes in which cold SSTS have persisted from July to October. This enhancement is due to a decrease in planetary boundary layer (PI]],) height[8] and/or near-surface PBL stabilization, both of which would lead to increased stress-divergence, and hence, enhanced damping of the near-surface ffow. The increased ε_u and ε_v will result in attenuation of both u and v, but the impact is greater on u as the 4°S- EQ averaged v is nearly zero to begin with in the cold-tongue longitudes. Composite atmospheric soundings over cool and warm eastern-Pacific SSTS, displayed in Figs. 5 and 6, respectively, in Bond (1992), graphically depict the near-surface PBL stabilization due to decrease of the underlying SS"1's.

In summary, we find the annual-cycle related $(SST)_x$ and zonal winds in the cold-tongue's core region to be related as envisioned in the LN-hypothesis [: $u \propto (SST)_x$]. A *visual* assessment of the validity of this hypothesis can be obtained by noting the correspondence between the (SS'1'), and u fields in the 130"W- 85"W sector in Jul y, and the 160°W- 85"W sector in October. The correspondence in July is, indeed, remarkable both in phase and amplitude, but the amplitude

---

[7]The difference between July and October easterly-wind strengths in the 135 °W–125°W sector, where the July (SS3'), forcing and meridional winds are nearly identical to those in October. is quite intriguing.

[8]The Rayleigh friction coefficients depend inversely on PBL height (H_0), whereas the SST-gradient driven sca-level pressure-gradients in the Lindzen-Nigam model are linearly dependent on HO. The sensitivity of the PBL flow to a ⅓ reduction in HO, discussed in Section 4 in Lindzen and Nigam (1987), consists primarily of a ⅓ reduction in u, and little (≤ 5%) change in v,

correspondence in October is not as striking due to the zonal variations in ε_u (and ε_v) that result from variations in PBL height, as discussed above.

B. The meridional momentum balance

We next examine the forcing of meridional winds at 100 °W---a longitude that is well within both the nascent and mature phases of the Pacific cold-tongue, and one where meridional and zonal winds are rather typical of the flow in the 130°W--90°W sector. Fig. 5 shows (f*u), v, SST, and $(SST)_y$ as a function of latitude during both July and October, just as in Fig. 4.

The off-equatorial expansion of the SST cold-tongue from July to October, with strongest cooling occurring in the southern latitudes, is clearly evident in the third panel. The central latitude is at 10S in July and close to 3°S in October; the meridional wind however vanishes (or is a minimum) at 3°S and 5°S, respectively, i.e., about 2° southward of the $(SST)_y$=0 latitude, in both these months. This variance from the I.N-hypothesis can be alternatively viewed by noting the non-collocation of $(\partial v/\partial y)_{max}$ and $(SST)_{min}$, for if $v \propto (SST)_y$, as in 1.N-hypothesis, then $(\partial v/\partial y)_{max}$ must be located where $(SST)_{yy}$ is maximum, or where SSTS arc a minimum. The meridional divergence is maxitnum at -4°N in July, and at -1 'N in October, i.e., about 4° northward of the expected latitude in both months, The meridional wind is similarly maximum not where $(SST)_y$ is maximum, but about 4° northward, at 7°N and 5°N in July and October, respectively. Most of the above noted departures from the '$v \propto (SST)_y$ structure' hypothesis can be summarized as the general tendency of the. meridional wind *speed* to be biased towards the warmer neighboring SSTS.

The reasons for the non-collocation of latitudes of $(\partial v/\partial y)_{max}$ and $(SST)_{min}$ in the equatorial eastern Pacific have been investigated by Wallace et al. (1989), and, more recently, by Bond (1992) whose analysis was briefly discussed in the preceding subsection. These studies indicate

that, in addition to the controlling influence of SST-gradients, the near-surface static stability variations (forced by SST-gradients, too) play an important role in modulating surface-wind *speed* through their impact on PBL height--for example, as one moves northward across the northern SST-front [: where $(SST)_y$ is maximum], the near-surface destabilization leads to an increase in the vertical range over which horizontal-momentum dissipation occurs, and therefore to reduced &v, and hence, greater v and $(\partial v/\partial y)$ over these latitudes, This aspect of SST-forcing is potentially parameterizable in the LN-model (by making ε_u and ε_v dependent on SS7's).

In summary, $v \propto [(SST)_y]/\varepsilon_v$ with ε_v dependent on SSTs, is a better approximation than $v \propto (SST)_y$. Note, however, that the PBL static-stability variation argument, which helps in understanding amplitude-modulation, cannot explain the meridional flow structure across the southern SST-front (-5°S) in July, as even the flow-direction there is at variance with the LN-hypothesis[9]

C. Role of zonal . vs. meridional winds in eastern Pacific annual-cycle evolution

Mitchell and Wallace (1992) have analyzed the annual variability of SS"1"s, surface winds and Outgoing Longwave Radiation (OLR), and found the meridional winds associated with the continental monsoons to play a central role in, at least, the initial expansion (till -120°W) of the cold-tongue. Their conclusions in this regard are essentially based on *a)* noting the similarity in the structure of SST-reduction occurring southward of the intensifying northward flow in the 0°- 5*N band during June/July, with the SST-reduction patterns obtained in ocean-modeling experiments (e.g., of Philander and Pacanowski, 1981 b) in response to northward wind stress

[9]Although the meridional wind at the southern SST-front is not from the north, it is nonetheless minimum there, The reduced sensitivity y of meridional wind to (SST), variations in these southern latit udcs (and at 100°W) results, perhaps, from the positive. feedback interaction of the Iow-level stratus decks and SSTs that leads to rather shallow boundary layers in this region (Mitchell and Wallace, 1992).

forcing at the northern edge of the equatorial waveguide, and *b)* and on noting the phase lead/lag of monthly-mean zonal (meridional) winds w.r.t. SSTs in the 4°S–4°N latitude (104 °W–86°W longitude) band.

It would be difficult to remark on the suitability of their *first* argument in this diagnostic study. It is sufficient to note here that, although, Mitchell and Wallace base their conclusion partly on it, they caution the reader against a ready acceptance of their first argument by citing a number of other ocean-modeling studies (e.g., Busalacchi and O' Brien, 1980; Takeuchi, 1988) that demonstrate the importance of the annual-march of zonal wind stress in accounting for the SST annual-cycle in the equatorial eastern Pacific.

Mitchell and Wallace's second argument is based on diagnostic analysis, and as such, can be analyzed here. Using longitude-time diagrams (their Fig. 12)'0, Mitchell and Wallace find that easterly-tendency does not temporally lead the cooling at the equator except near 120°W—such a lead would be critical to arguments advancing the importance of zonal-wind changes in the *initiation* of cooling along the equator. We re-examine the temporal evolution of annual-cycle variability, as captured by the two-leading combined modes (Figs. 1 and 2), in the 4°S–EQ latitude band in Fig. 6. Examination of this figure reveals that:

- In the coastal zone (eastward of 100°W), SST-cooling begins in April, when there exists, essentially, a southerly surface-wind *tendency in* this sector. 'I'he easterly-tendency in the coastal longitudes occurs far too early in the year (December–January) to be plausibly connected with the April coastal cooling. Given this, there is little doubt that SST-cooling in the coastal zone is initiated by the slackening of local northerly winds in April. An inspection of the timings

[10]This figure is based on COADS monthly-mean climatology of zonal wind-stress and SS1's, but as the annual-means arc not subtracted out, discerning temporal phase lead/tag between these two fields is, difficult, particularly, in the equatorial eastern Pacific.

of maximum-SSTs and maximum-northerlies in Fig. 6 indicates, perhaps, a half-month lead of meridional wind changes in the coastal zone.

► Beyond the coastal zone (westward of 100°W), SST-cooling begins in April too, but this time there exists robust easterly and modest southerly surface-wind *tendencies in* this sector. The southerly wind-tendency in this sector is not only weak, but also likely to be ineffective in modulating upwelling, and hence SSTS, far away from a north-south coast. The April SST-cooling in this sector must therefore result from the Ekman generated equatorial upwelling that is forced by the March-onwards slackening of local westerlies.

There is, thus, evidence that surface *zonal*-wind changes play a rather important role in engendering the warm-to-cold phase (and vice-versa) transition of the ocean-atmosphere annual-cycle in the off-coastal longitudes (westward of 100°W) of the equatorial eastern Pacific. Mitchell and Wallace have discounted the role of zonal windstress changes in engendering annual-cycle related SST-changes, in part, through their observation that "Farther to the west (of 120°W), the increase in stress (westward) is observed too late in the year to account for cooling during Phase I (March- to-May)." While it is true that the easterly-tendency at 140°W is most pronounced during June--August (see Fig. 6), i.e., two months after the initiation of coastal cooling, this easterly-tendency still *leads* the SST-cooling *at this longitude.* The *local* temporal lead/lag relationships are, perhaps, more germane for understanding the mechanism governing tropical ocean-atmosphere annual-cycle variability. The above-noted phase-relationships of zonal and meridional surface winds with SSTS, while most pronounced in the 4°S- EQ band-averages, are clearly evident also in wider latitude-bands that are centered on 2°S (e.g., the 6°S- 2“N band).

Finally, one must ask how the annual-cycle variability, obtained by summing the two annual-cycle modes extracted from an RPCA analysis of combined tropical ocean-atmosphere

variability, compares with that obtained by calculating the departures of the climatological monthly-means from the annual-mean? Results of the latter calculation with COADS '4 °S- EQ' averaged data are displayed in Fig. 7 in a format identical to that of Fig. 6. Comparison of these two figures indicates remarkable similarity in SST-evolution except for the somewhat stronger amplitudes and somewhat more extended westward propagation of warm-phase SSTs in Fig. 7. The amplitude-asymmetry between the annual-cycle's two phases is however striking in the surface-wind evolution panels of Fig. 7, indicating, perhaps. the presence of sub-annual harmonic and/or aliased variability in the COADS's climatological monthly-mean departure (from the annual-mean) fields---such variability components are separated out in the undertaken RPCA analysis even though that analysis was based on the spatial-recurrence criterion alone. 'l'he inadvertent presence of sub-annual harmonic and/or aliased variability in a 'climatological monthly-mean based' annual-cycle variability analysis (e.g., of Mitchell and Wallace, 1992, or Fig. 7 of this study) also distorts some of the above-noted temporal phase lead/tag relationships (compare Figs. 6 and 7) that are revealing of the dynamics governing the coupled ocean-atmosphere annual cycle in the eastern Pacific.

D.The west ward expansion hypothesis

The analysis of zonal and meridional momentum balance across the nascent and mature phases of the Pacific cold-tongue, presented in section 6A and 6B, shows the equatorial wind, and, in particular, its zonal component to be dynamically consistent with the cold-tongue related SST-gradients. An examination of the annual evolution of zonal and meridional winds and SS"1's, moreover, indicates the importance of zonal-wind changes in generating SST-changes in the Pacific off-coastal longitudes (westward of 10OOW). Taken together, these findings, suggest the following equatorial air-sea interaction scenario for the westward expansion of the cold-tongue:

➤ The zonal SST-gradient is negative at the leading edge and positive at the trailing edge of the cold-tongue during July (cf. Figs. 1 & 4), The generation of negative zonal SST-gradients at the leading edge is significantly aided by the June-to-July presence of warmer SSTS in the equatorial central Pacific (1 800–120"W) that have been noted before in Figs. 1& 3.

➤ The zonal wind forced by these 'SST-gradient driven' sea-level pressure gradients should be maximum easterly (westerly) at the leading (trailing) edge of the cold-tongue, or more precisely, where SST-gradients are minimum/maximum. As noted in discussion of Fig. 4 above, the longitudinal structure of both July and October zonal winds and SSTS in the 4°S- EQ band is quite consistent with the 'SST- zonal wind' phase-relationship suggested by the LN-hypothesis.

▸ The easterlies at the cold-tongue's western edge generate colder SSTs *there* through Ekman-pumping driven equatorial upwelling- -such equatorial air-sea interaction via which colder SSTS arc successive y generated at the western edge of the old ones, leads to the westward *expansion* of the cold tongue[11].

▸ In view of the above discussed enhancement of Rayleigh friction coefficients (ε_u and ε_v) due to PBL stabilization over expanding colder waters, the easterlies slacken behind the leading edge of the cold-tongue, leading to moderation of equatorial upwelling there, and this, perhaps, limits the coldest SSTS that can be generated in the cold-tongue's core region.

▸ The westward expansion of the cold-tongue occurs till October/November when its leading edge is close to 160°W. l-he above described equatorial air-sea interaction terminates at -160°W because the zonal wind in its vicinity is no longer proportional to $(SST)_x$, as evident from Fig. 5. This lack of proportionality between u and $(SST)_x$, when both are quite small, as

[11]The easterly surface winds to the west of the cold SSTs should also, advectively, facilitate the westward expansion of the cold tongue.

near 160°W, is not surprising in view of the everpresent "free" component of the pressure field, and its relatively more significant impact on surface winds in such 'SST-gradient devoid' regions. But why are the generated zonal SST-gradients in this equatorial central Pacific region so weak? "r'he answer to this, perhaps, resides in the second-order attenuation of Ekman-driven entrainment, resulting from the rapid westward deepening of the annual-mean thermocline across the longitudes in question,

The demise of SST cold-tongue occurs in an equally interesting manner, and is initiated by the weakening of along-shore southerlies in the equatorial eastern Pacific in November. This slackening of the along-shore southerlies, relatable to the transition between northern and southern summer monsoonal flows, leads to reduction in coastal upwelling and consequent weakening of the cold-tongue; a nascent warm-tongue, in fact, appears in the equatorial eastern Pacific at, as early as, December's end, as evident from the display of the extracted SST annual-cycle variability in the bottom panel of Fig. 3.

The westward expansion of the SST warm-tongue during January to April proceeds in much the same manner as the above described expansion of the cold-tongue, and is again aided, initially, by the presence of oppositely-signed (cold) SSTs in the equatorial and south-equatorial central Pacific in the November-January period (Fig. 3). A warm SST anomaly in the equatorial eastern Pacific should generate westerlies (easterlies) at its western (eastern) edge if sea-level pressure gradients are determined largely by the local SST-gradients. Equatorial air-sea interaction will again lead to westward expansion; this time, however, surface westerlies at the western edge of the warm SS'1s will not advectively aid the westward expansion of warm SSTs.

E. Robustness of the observational bases for the westward expansion hypothesis

The westward expansion hypothesis, developed in subsection 6D, was based on the

analysis of zonal and meridional momentum-balances along the 4°S–EQ band and along 100"W, respectively, during both July and October. In this section, we ascertain the robustness of the observational bases for the proposed westward expansion hypothesis by examining the evolution of annual-cycle variability (: RLV1 +RLV2) in the 6°S–20N latitude-band in Fig. 8.

The westward expansion hypothesis is based on the following two observations: First, that the easterly-tendency temporally leads *local* SST-cooling in the off-coastal longitudes of the cold-tongue's core region, which is equivalent to the zonal wind leading the SS'1's at these longitudes. The phase-lead in monthly-units (δ), with $0<\delta<6$, can be estimated from the temporal distance of u and SST nodal lines in the evolution diagrams. An inspection of Fig. 8 shows that even in this 8° wide latitude-band, the zonal winds lead SS'1's in the off-coastal eastern Pacific longitudes, and that the phase-lead (δ) is about a month in the 140"W- -1 10"W sector.

The second observational basis for this hypothesis is that the zonal pressure-gradients in the cold-tongue's core region are thermodynamically consistent with the zonal SST-gradients (the I.N-hypothesis), i.e., $p_x \propto -(SST)_x$. This, together with the discussion of zonal-momentum balance in section 6A, suggests that $u \propto [(SST)_x]/\varepsilon_u$, or that zonal wind and SSTs are out-of-phase by a quarter zonal-wavelength, with the zonal-wind leading the SSTs. The corroborative search for such a relationship in the 140°W–80°W sector in Fig. 8 is, perhaps, best conducted by noting the zonal lead/lag of nodal lines (and not of the extremums) in view of the modulation of zonal-wind amplitudes from ε_u's dependence on SS'l-s (see section 6A). An inspection of Fig. 8 reveals that the quarter zonal-wavelength phase-difference noted between u and SSTS in the 4°S–EQ band in Fig. 4, is also present in the '6 °S--20N latitude-band averaged' u and SS'1's; in both instances, u leads the SSTs—in accord with the I.N-hypothesis. Consider, for example, the zonal winds at the end of September, when u has a node in the eastern Pacific at ~95°W just where

the SSTS are a minimum [and, therefore, $(SST)_x \approx 0$]; further to the west, the easterlies are maximum at -120°W, precisely, where $(SST)_x$ is maximum-negative.

In summary, we find broad validity of the observational bases upon which the westward expansion hypothesis is founded. The undertaken analysis of annual-cycle variability indicates that easterly-tendency leads SST-cooling in the off-coastal longitudes by about a month. Such time-delay in the SST-response is in accord with Neelin's (1991) estimation of the Ekman-driven equatorial-upwelling response time-scale from anomalous upwelling of mean temperature gradients, which is also -1 month.

F. Semi-annual cycle in the eastern Pacific

The sub-annual harmonic and/or aliased variability obtained by compositing the variability represented by the eight-leading '*non* annual-cycle' modes (RLV3–RLV10)[12] extracted from an RPCA analysis of combined variability, is displayed in Fig. 9. This variability is evidently dominated by the semi-annual component which is ultimately forced by the semi-annual cycle in solar-declination within ±23.5° of the equator. A comparison of Figs. 9 and 6 shows a nearly complete semi-annual cycle spanning any one phase of the annual-cycle, The skewness in semi-annual warm-phase amplitudes between March--May and September-November likely results from the second-order influence of the SST annual-cycle.

"l'he evolution of semi-annual variability is quite reminiscent of the annual-cycle evolution discussed earlier, in that, coastal meridional winds are nearly out of phase with the coastal SS1's; interestingly, the ratio of SST-to-meridional wind amplitudes along the South American coast is

[12]The 38-year long coefficient lime-series of each RLV was processed just as the COADS data that generated Fig. 7, and then multiplied with the corresponding RLV. Virtually all of the low-frequency variability is contained in the first-ten modes, for their SUM (Fig. 6 plus Fig. 9) is indistinguishable from Fig. 7. RLV3 and RLV4 are El Niño related interannual variability modes whose structure/dynamics is discussed in a separate paper,

-1 both in case of semi-annual and annual-cycle variability. Although, northerly winds barely lead the warm SSTS along the Pacific coast, they appear central to the generation of warm coastal SSTS (via Ekman downwelling) in view of the rather weak zonal-wind tendencies there, and that too, easterly, in the months prior to the peak warming in March/April. As before, the zonal-wind changes appear to be important in generating SST-changes in the off-coastal longitudes, e.g., the easterly-wind tendency, which is maximum at the nodal line of u, leads SST-cooling by about a month in the 140 °W---1000W sector. The slopes of SST nodal lines in this sector are however not as steep as those in Fig. **6,** indicating faster westward propagation of the semi-annual SST-phase--for reasons not understood at the present time.

7. Evolution of the Atlantic SST cold-tongue

The Atlantic seasonal-cycle evolution is quite similar to that in the eastern Pacific as evident from an examination of surface-winds and SST structures in the two-leading annual-cycle variability modes (Figs. 1 and 2). At the peak of the 'monsoonal mode' (i.e., July), both the SST cold-tongues are coastally-connected in the southern tropics, have their central latitude at -2°S, and have similar longitudinal extent (which in case of the Atlantic cold-tongue, is almost the entire tropical Atlantic basin). The notable differences between them include the stronger amplitude of the Atlantic cold-tongue, and the absence of a sharp equatorial SST front at its northern flank. During October, when the 'monsoonal mode' is changing phase (i.e., going through a zero-crossing) and the second annual-cycle mode (Fig. 2) is at its peak, the Pacific cold-tongue is more robust, and because of basin-size considerations, more zonally and meridionally extended too.

The Atlantic annual-cycle evolution is however not synchronous with the eastern Pacific annual-cycle evolution, as revealed by the longitude-time display of extracted annual-cycle

variability in the 4°S–EQ latitude band (Fig. 6) or in the 6°S–20N band (Fig. 8). The SST evolution in the Atlantic leads by at least a month--- the coastal cooling begins in mid-February, albeit weakly, but gathers momentum only in April when SST-cooling is evident across most Atlantic longitudes. Prior to the concerted April cooling, the surface winds exhibit an easterly-tendency both in the coastal sector (0°–10°E) as well as in the central Atlantic (20 °W- 0°), and essentially a southerly-tendency further to the west. The phase-lead of such surface-wind tendencies indicates, as before, the importance of equatorial air-sea interaction of zonal-winds and $(SST)_x$ in promoting the westward propagation of SST-phase across the eastern and central Atlantic. The SST-evolution in the western Atlantic is more difficult to understand due to the presence of a northwest-to-southeast oriented coastline.

8. **SST annual-cycle in the Indian Ocean**

The SST annual-cycle amplitudes in the equatorial Indian Ocean are only about one-fifth of those in the eastern Pacific and Atlantic (see Fig. 3), but their evolution is notable because of an apparent eastward propagation of SST-phase across most Indian Ocean longitudes. An examination of surface winds and SSTS associated with the seasonal (July) onset of Asian summer-monsoon (Fig. 1) however reveals the zonal wind (and SSTs) to reverse phase across the 5°S–EQ band in the Indian Ocean longitudes, which suggests that annual cycle evolution in the Indian Ocean should be analyzed, separately, in the northern and southern equatorial basins. We focus here on the northern equatorial basin because of its proximity to both Asia and Africa, and annual-cycle variability in this region is displayed in Fig. 10 via the 2°N–60N band-averages.

The annual evolution of zonal and meridional surface winds in the northern equatorial Indian ocean is so similar in the off-coastal longitudes that the surface momentum balance there must be: $\varepsilon_u u \approx f_{4°N}\, v$, and $\varepsilon_v v = -f_{4°N} u - p_y / \rho_o$, *with* $\varepsilon_u \approx f_{4°N}$ [or $-(1.2\ \text{days})^{-1}$] in the eastern

Indian Ocean. This ε_u value is similar to that diagnosed from a more careful analysis of surface momentum balance over the equatorial central/eastern Pacific (e.g., Deser, 1993). The phasing of SSTs w.r.t. meridional (or zonal) winds along the Somali coast is such that southwesterly winds (part of the low-level Somali jet) lead cold S STS by about a month, with the wind-lead increasing eastward in the off-coastal longitudes (50°E–65°E).

While the SST-lag of about a month along the Somali coast can be attributed to the Ekman-driven coastal upwelling response time, the greater SST-lag in off-coastal longitudes is more difficult to understand. As SSTS in the off-coastal and off-equatorial oceans that are warm in the annual-mean (like the northern equatorial Indian Ocean) change also in response to surface wind-*speed* variations, which modulate both the latent-heat flux as well as vertical stirring of the oceanic mixed layer, the surface wind-speed variability[13] associated with the annually evolving surface winds is also shown in Fig. 10 to facilitate understanding of the SS'1" annual-cycle in this oceanic region[14].

The surface wind-speed in off-coastal longitudes begins increasing in April, and attains maximum amplitude at the end of July; the July wind-speed is largest at ~85°E and smallest at ~65°E. If the wind-speed variations controlled SSTS (through changes in latent-heat flux and vertical stirring), the above *zonal* variation in wind-speed increment would initiate gradual cooling at ~65°E, and rapid cooling at ~85°E, both as observed in the SST-panel of Fig, 10, The surface wind-speed is most intense at the end of July at which time the SST-cooling is also most

[13]Surface wind-speed variability, also displayed in Fig.] O, is the departure of *total* wind-speed (: speed of the sum of annwd-mean and annual-cycle components) from its annual-nun value. As such, it will contain *non* annual-cycle frequencies as well, as evident from its evolution in Fig. 10.

[14]Surface wind-speed variability should have limited impact on coastal SSTs which are largely determined by coastal upwelling/downwelling; this assessment is, indirectly, confirmed by noting the presence of semi-annual cycle variability in coastal surface wind-speed, but none in coastal SST-variability.

vigorous; the coldest SSTS are however realized about 1--2 months later, both at 65°E and 85°E. The reduction in wind-speed in the July onward period should, by the same reasoning, lead to SST-warming, but examination of SST-evolution indicates that the warming does not commence until December, perhaps, because of the opposing impact of insolation forcing in this period.

In summary, the annually-evolving surface winds and SSTs in the northern equatorial Indian Ocean basin *do not* appear to be dominantly governed by the coupled ocean-atmosphere dynamics that explained, reasonably successfully, the notable aspects of annual-cycle variability in the equatorial eastern Pacific and Atlantic. Instead, modulations of latent-heat flux and oceanic mixed-layer stirring due to robust 'surface wind-speed variability' (amplitude of ~3 m/s) appear important in producing the modest SS"1' annual-cycle (amplitude of ~0.5°K) observed in off-coastal longitudes. It is important to note that the governing dynamics, in case of the northern equatorial Indian Ocean, is quasi-uncoupled, in that, surface-wind variability is forced by seasonal monsoons, and not by interactions with the local underlying SS1's (as in the other two equatorial eastern ocean basins).

9. **Discussion and Conclusions**

This study has attempted to contribute to the elucidation of the dynamics governing the most fundamental aspect of coupled seasonal-climate evolution in the eastern equatorial ocean basins--the westward/northward expansion of the SST cold-tongue during northern summer and autumn. This contribution consists, first, of objective extraction of the combined structure of ocean-atmosphere annual-cycle variability from the 1950--1987 COADS month] y-mean surface-wind and SSTS, and shallow-water model simulated ocean-heat content, and, secondly, and more importantly, of dynamical diagnostic analysis of the extracted annual-cycle variability to reveal the underlying coupled dynamics.

The RPCA analysis, based on the spatial-recurrence criterion alone, was rather successful in separating the combined ocean-atmosphere variability into annual, semi-annual and interannual variability components. This method of extraction of annual-cycle variability is preferable to the canonical method based on departures of climatological monthly-means from the annual-mean, for semi-annual and aliased interannual-variability are not separated out via the latter method.

The coupled annual-cycle variability is compactly describable using *two* modes that are in temporal quadrature, and whose structures are insensitive to the inclusion/exclusion of oceanic heat-content in the combined variability analysis. The *first* mode, peaking in July (and January), represents large-scale monsoonal flow onto the warmer continents: Indo-China, Central America, and western Africa. The *second* annual-cycle mode peaks in October (and April) when it represents the extreme phases of SST annual variability in the eastern oceans.

An analysis of zonal and meridional momentum-balances associated with the annual-cycle related surface-winds in the Pacific cold-tongue's core region shows the equatorial flow, and, in particular, the zonal-wind component, to be dynamically consistent with the 'SST-gradient driven' sea-level pressure gradients (Lindzen and Nigam, 1987) during both the cold-tongue's nascent (July) and mature (October) phases. Although the longitudinal phase-relationship between annual -cycle zonal winds and SSTS is rather consistent with that expected from the Lindzen-Nigam hypothesis [: $u \propto (SST)_x$], the amplitude relationship is at some variance unless the impact of near-surface static-stability variation (due, ultimately, to the underlying SST variations, and therefore parameterizable) on horizontal-momentum dissipation is factored in. In summary, $u \propto [(SST)_x]/\varepsilon_u$ and $v \propto [(SST)_y]/\varepsilon_v$, with ε_u and ε_v dependent on SSTS, are better approximate descriptors of the surface flow in the cold-tongue's core latitudes and longitudes than $u \propto (SST)_x$ and $v \propto (SST)_y$.

An examination of the annual evolution of zonal and meridional winds and SSTS in both

4°S–EQ and 6°S–2°N band-averages reveals the easterly zonal-wind tendency to lead local SST-cooling both in the off-coastal eastern Pacific (140°W–1OO°W) and in the central/eastern Atlantic (2O"W-1O"E) by about a month. On the basis of the above-noted spatial and temporal phase-relationships between zonal wind and SSTS in the cold-tongue's core-region, an equatorial air-sea interaction hypothesis is proposed to explain the westward expansion of *both* warm and cold-phase SSTS in the off-coastal equatorial eastern oceans. (As noted before, SST-changes in the South American coastal zone are initiated by the slackening of local along-shore winds.) The salient features of the 'westward expansion hypothesis' in Pacific cold-tongue development are:

➤ SST-cooling (from reduced downwelling), initiated by slackening of the alongshore April northerlies, generates negative (SST), at the western edge of the coastal zone.

➤ 'SST-gradient driven' sea-level pressure gradients force maximum easterlies where $(SST)_x$ is maximum-negative, i.e., along the western edge of the coastal zone.

➤ Easterlies at the 'maximum-negative SST-gradient' site (: westward of the coldest SSTs) generate colder SSTS *there* through Ekman-pumping driven equatorial upwelling—such equatorial air-sea interaction via which colder SSTs are successively generated westward of the previously coldest ones, leads to westward *expansion* of the cold tongue.

➤ Westward expansion of the cold-tongue continues till its leading edge is at -160"W— a region where only modest (SST), can be generated due to the second-order attenuation of Ekman-driven entrainment from rapid westward deepening of the annual-mean thermocline in this region.

The proposed 'westward expansion hypothesis' appears to have some similarity with the dynamics of the 'slow SST mode' (Neelin, 1991), although the latter has thus far been shown to be a useful concept in understanding, primarily, the longer-period ocean-atmosphere variability (e.g., ENSO related interannual variability). Whether dynamical results obtained in the 'fast-wave

limit' are applicable to annual-cycle variability issues is uncertain. Nonetheless, it is instructive to note that the two processes whose coupling constitutes the 'westward expansion hypothesis', namely, atmospheric PBL dynamics/thermodynamics that yields $u \propto (SST)_x$ [Lindzen and Nigam, 1987], or better yet, $u \propto [(SST)_x]/\varepsilon_u$, *and* Ekman ocean mixed-layer dynamics, are also integral components of the coupled dynamics that leads to westward propagation of the 'slow SST mode'.

This study also finds that

▸ evolution-dynamics of semi-annual variability in the equatorial eastern Pacific is strikingly similar to that controlling annual-cycle variability, except for the somewhat faster westward propagation of SST-phase in the former,

➤ SST annual-cycle evolution in the Atlantic basin leads the eastern Pacific SST annual-cycle by at least a month, and that in the eastern Atlantic coastal zone, zonal-wind tendencies play a more prominent role in promoting SST-changes (in at least the 4°S–EQ band), and

▸ that in the northern equatorial Indian Ocean, modulations of latent-heat flux and oceanic mixed-layer stirring due to robust 'surface wind-speed variability' (amplitude of ~3 m/s) appear important in producing the modest off-coastal SST annual-cycle (amplitude of ~0.5°K).

Although encouraging, the present study leaves several questions unanswered, many of which can be probed only by modeling experiments with controlled physics and/or dynamics. Among them are questions such as:

▸ What, if any, is the role of annually-varying ocean-atmosphere heat-fluxes in controlling the pronounced annual cycle in the eastern ocean basin?

▸ What is the mechanism governing the northward expansion of the SST cold-tongue?

The principal question for modeling studies remains whether the equatorial eastern Pacific SSTs respond primarily to local or remote wind stress forcing.

Acknowledgments

This work was supported by NOAA Grants NA26GP0116 and NA46GP0194 to S. Nigam at the University of Maryland, College Park, and by NASA Grants UPN578-21-23 and UPN 578-21-24 to Yi Chao at the Jet Propulsion Laboratory. Preliminary findings of this study were presented at the American Geophysical Union's Fall Meeting in December '93 in San Francisco,

S. Nigam would like to thank Deng-Hua Wu, James Carton, and Chul Chung, all at the University of Maryland for helpful discussions, and NOAA Program Manager, Dr. Ken Mooney, for his continued support of climate-diagnostic research.

" REFERENCES

Bond, N. A., 1992: observations of planetary boundary -layer structure in the eastern equatorial Pacific. *J. Climate, 7, 699-706.*

Busalacchi, A.J., and J.J. O'Brien, 1980: The seasonal variability in a model of the tropical Pacific. *J. Phys. Oceanogr.*, **10,** 1929-1951.

Chang, P., and S. G. H. Philander, 1994: A coupled ocean-atmosphere instability of relevance to seasonal cycle. Submitted to *J. Atmos. Sci.*

Chao, Y., D. Halpern, and C. Perigaud, 1993: Sea surface height variability during 1986-1988 in the tropical Pacific ocean. *J. Geophys. Res., 98, 6947-6959.*

Chao, Y., 1990: Seasonal and interannual variability in the tropical Pacific ocean. Ph.D. dissertation, Princeton University, Princeton, NJ.

Da Silva, A. M., C.C. Young, and S. Levitus, 1993: A method for correcting Beaufort estimated winds in COADS. Submitted to *J. Appl. Meteor* (pending revision).

Deser, C., 1993: Diagnosis of the surface momentum balance over the tropical Pacific ocean. *J. Climate, 6, 64-74.*

Horel, J. D., 1982: The annual cycle in the tropical Pacific ocean and atmosphere. Mon. *Wea. Rev.*, 110, 1863-1878.

Lindzen, R, S., and S. Nigam, 1987: On the role of sea-surface temperature gradients in forcing low-level winds and convergence in the tropics. *J. Atmos. Sci.*, 44, 2418-2436.

Mitchell, T, P., and J.M. Wallace, 1992: The annual cycle in equatorial convection and sea surface temperature. *J. Climate, S, 1140-11* S6.

Neelin, J. D., 1991: The slow sea surface temperature mode and the fast-wave limit: Analytic theory for tropical interannual oscillations and experiments in a hybrid coupled model. *J. Atmos. Sci., 48, 584-606.*

Nigam, S., and H.-S. Shen, 1993: Structure of oceanic and atmospheric low-frequency variability

over the tropical Pacific and Indian oceans. Part-I: COADS Observations. *J. Climate, 6, 657-676.*

Philander, S. G. H., and R.C. Pacanowski, 1981a: The response of equatorial oceans to periodic forcing. *J. Geophys. Res., 86,* 1903-1916,

Philander, S. G. H., and R.C. Pacanowski, 1981b: The oceanic response to cross-equatorial winds (with application to coastal upwelling in low latitudes). *Tellus,* **33,** 201-210.

Rasmussen, E. M., and T.H. Carpenter, 1982: Variations in tropical sea-surface temperature and surface wind fields associated with the Southern Oscillation/ El Niño. *Mon. Wea. Rev., 110,* 354-384.

Robertson, A. W., C.-C. Ma, C.R. Mechoso, and M. Ghil, 1994: Simulation of the tropical Pacific climate with a coupled ocean-atmosphere general circulation model. Part-1: Seasonal cycle. Submitted to *J. Climate.*

Ropelewski, C. F., and M.S. Halpert, 1987: Global and regional-scale precipitation associated with El Niño/ Southern Oscillation. *Mon. Wea. Rev., 11S,* 1606-1626.

Sadourney, R., 1975: Compressible model flows on the sphere. *J. Atmos. Sci., 32, 2103-2110.*

Takeuchi, K., 1988: Numerical study of the seasonal variation of the cold water tongue in the eastern tropical Pacific. *J, Fat, Sci. Hokkaido Univ., Ser. 7, 8, 221-241.*

Wallace, J.M., T.P. Mitchell, and C. Deser, 1989: "l'he influence of sea surface temperature on surface wind in the eastern equatorial Pacific: Seasonal and interannual variability. *J. Climate, 2, 1492-1499.*

Wang, B., 1992: On the annual cycle in the equatorial Pacific cold tongue. Submitted to *J. Climate.*

Weare, B. C., and J.S. Nasstrom, 1982: Examples of extended empirical orthogonal function analyses. Mon. *Wea. Rev.,* **110,** 481-485.

Wu, Deng-Hua, 1994: An investigation of air-sea feedbacks on the annual cycle in the tropical Pacific. Being submitted to the *J. Climate.*

FIGURE CAPTIONS

1. The leading recurrent mode of combined variability of COADS surface winds and SSTS, and simulated ocean heat-content (H_{con}), obtained from an RPCA analysis of two-month averaged (J+F, M+A, and so on) anomalies (from their respective climatological annual-means). The zonal and meridional surface-winds are shown in the top-two panels with a contour interval of 0.3 m/s, SST component with superposed surface-wind vectors in the third panel with a 0.2°K interval and a 5 m/s maximum vector, and H_{con} in the fourth panel with a 2.0 cm interval. The common coefficient time series, shown in the bottom-most panel, reveals this mode to be associated with annual-cycle variability. This mode, referred to as the 'monsoonal' mode, explains about 41 % of the combined domain-averaged variance of two-month averaged anomalies in the 1950- 1987 period. All contour maps are generated from 6°long. x 201st. fields, except for the wind-vectors which are plotted at 12 °long. x 401st. resolution,

2. The second-leading mode of combined variability of two-month averaged COADS surface winds and SSTs, and simulated H_{con} anomalies. It represents extreme phases of annual-cycle related variability in the eastern ocean basins, and explains about 19% of the combined domain-averaged variance. Rest as in Fig. 1.

3. The temporal evolution of the 4°S-EQ band-averaged SS"1'S in the two-leading annual-cycle related variability modes (top-two panels), and in their sum (bottom panel). These displays are obtained by multiplying the composite coefficient time-series (principal components) of each mode with the corresponding rotated loading vector. The contour interval and shading thresholds are 0.2°K in the top-two panels, and 0.4°K in the bottom panel, The month-markings are at the end of calendar months.

4. The longitudinal structure of July (open circles) and October (solid circles) annual-cycle related and '4"S–EQ band-averaged' surface winds (top-two panels), SSTS (third panel), and zonal

SST-gradients (bottom panel) to facilitate understanding of the zonal-momentum balance in the Pacific cold-tongue's core region.

5. 'I'he latitudinal structure of July (open circles) and October (solid circles) annual-cycle related Coriolis force (f*u) and meridional surface-winds (left-two panels), SSTS (third pane]), and meridional SST-gradients (right-most panel) to facilitate understanding of the meridional-momentum balance at a representative Pacific cold-tongue longitude (1 OO"W).

6. The temporal evolution of extracted total annual-cycle variability (: RLV1+RLV2) of the 4°S–EQ band-averaged SSTs and surface-winds in the eastern Pacific and Atlantic longitudes. The undertaken compositing is as described in the Fig. 3 caption. The contour interval and shading thresholds are 0.4°K in the SST-display, and 0.2 m/s in the surface-wind displays.

7. The temporal evolution of annual variability of COADS SS'1's and surface-winds, calculated from the departures of climatological two-month averages from their climatological annual-means. Rest as in Fig. 6.

8. As in Fig. 6, but for the 6°S–2°N band-averages,

9. The temporal evolution of the extracted '*non* annual-cycle' variability (: sum of RLV3 to RLV 10) of the 4°S–EQ band-averaged SSTS and surface-winds in the eastern Pacific and Atlantic longitudes. The undertaken compositing is as described in the Fig. 3 caption, The contour interval and shading thresholds are 0.1 'K in the SST-display, and 0,1 m/s in the surface-wjnd displays.

10. The temporal evolution of extracted total annual-cycle variability (: RLV1+RLV2) of the 2°N-6°N band-averaged SS"1's and surface-winds in the Indian Ocean longitudes. The undertaken compositing is as described in the Fig. 3 caption. "l'he right-most panel displays the evolution of associated surface wind-speed variability (see footnote 13 for more details). The contour interval and shading thresholds are 0.2°K in the SST-display, and 1.0 m/s in the other displays.

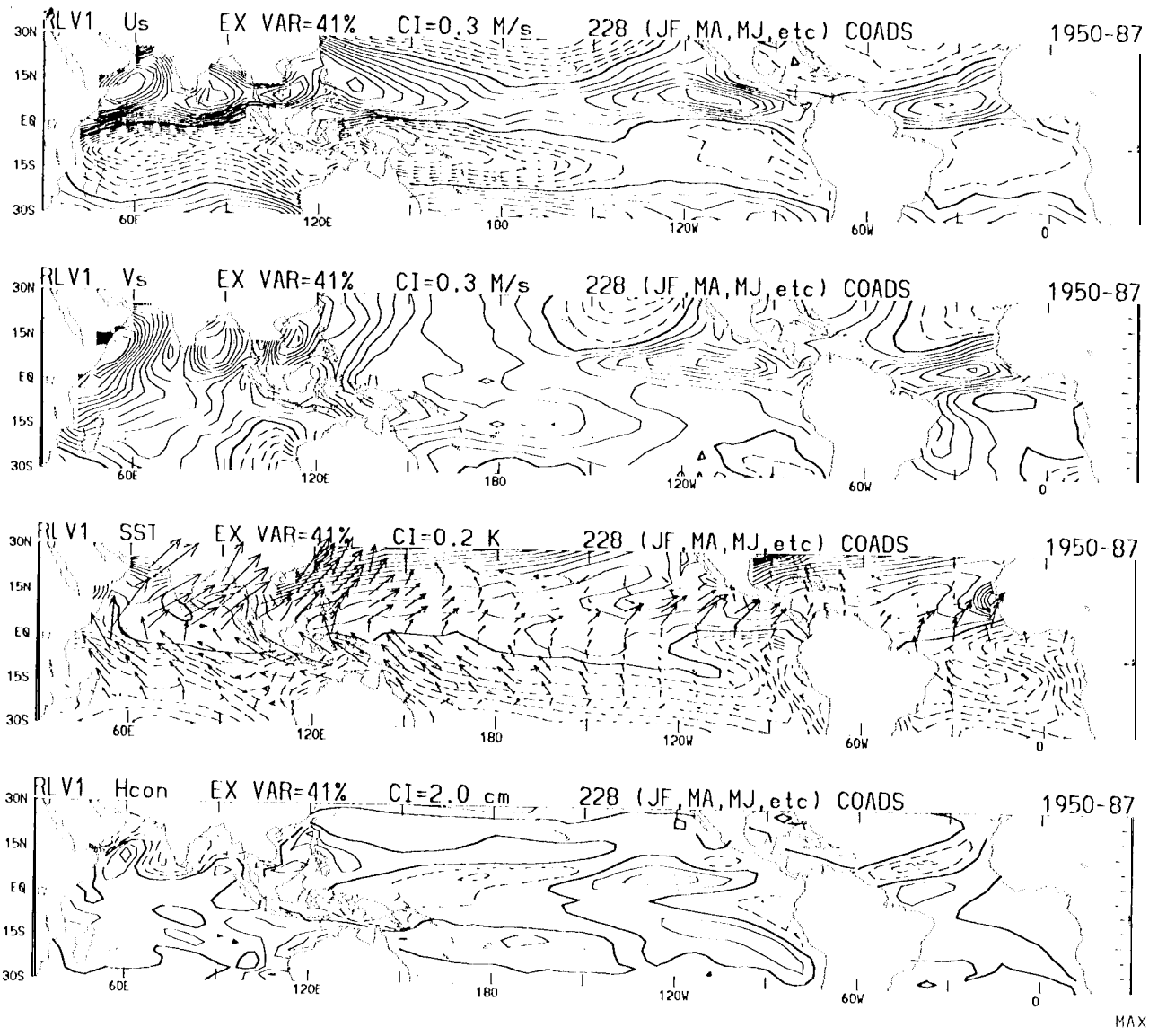

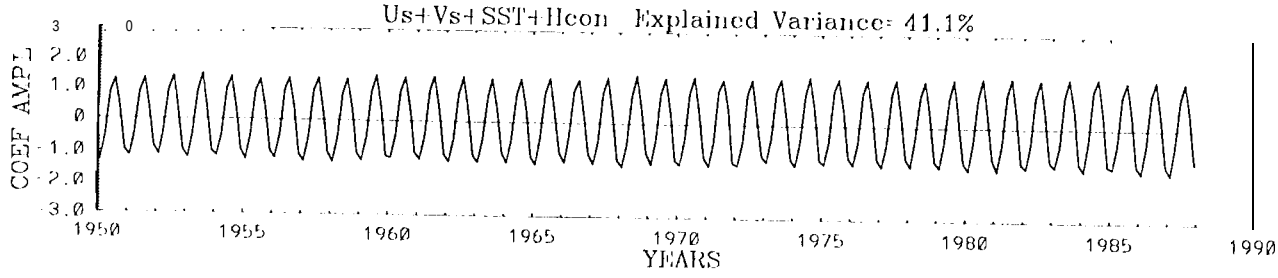

1. The leading recurrent mode of combined **variability of COADS surface winds and SS'1's, and simulated ocean heat-content (1** I_{con}**), obtained from an RPCA analysis of** two-month averaged (J+F, M+ A, **and so on) anomalies (from their** respective climatological **annual-means).** The zonal **and** meridional **surface-winds are shown in the** top-two **panels with a contour** interval of **().3 m/s, SS'1'** component **with superposed surface-wind** vectors **in the third pane.1 with a** 0.2°K **interval and a 5** m/s **maximum vector, and** H_{con} **in the fourth panel with a 2.() cm** interval. The common **coefficient** time series, **shown in the** bottom-most **pane], reveals this mode to** be **associated with annual-cycle variability. This mode,** referred to as the **'monsoonal' mode, explains** about **41 %** of the combined **dornain-averaged variance** of two-month **averaged anomalies in** the **19S()** 1987 period. **All contour maps at-c** generated **from** 6°long. x 2°lat. **fields,** except **for the, wind-vectors which arc** plotted **al 12** °long. x 4°lat. **resolution.**

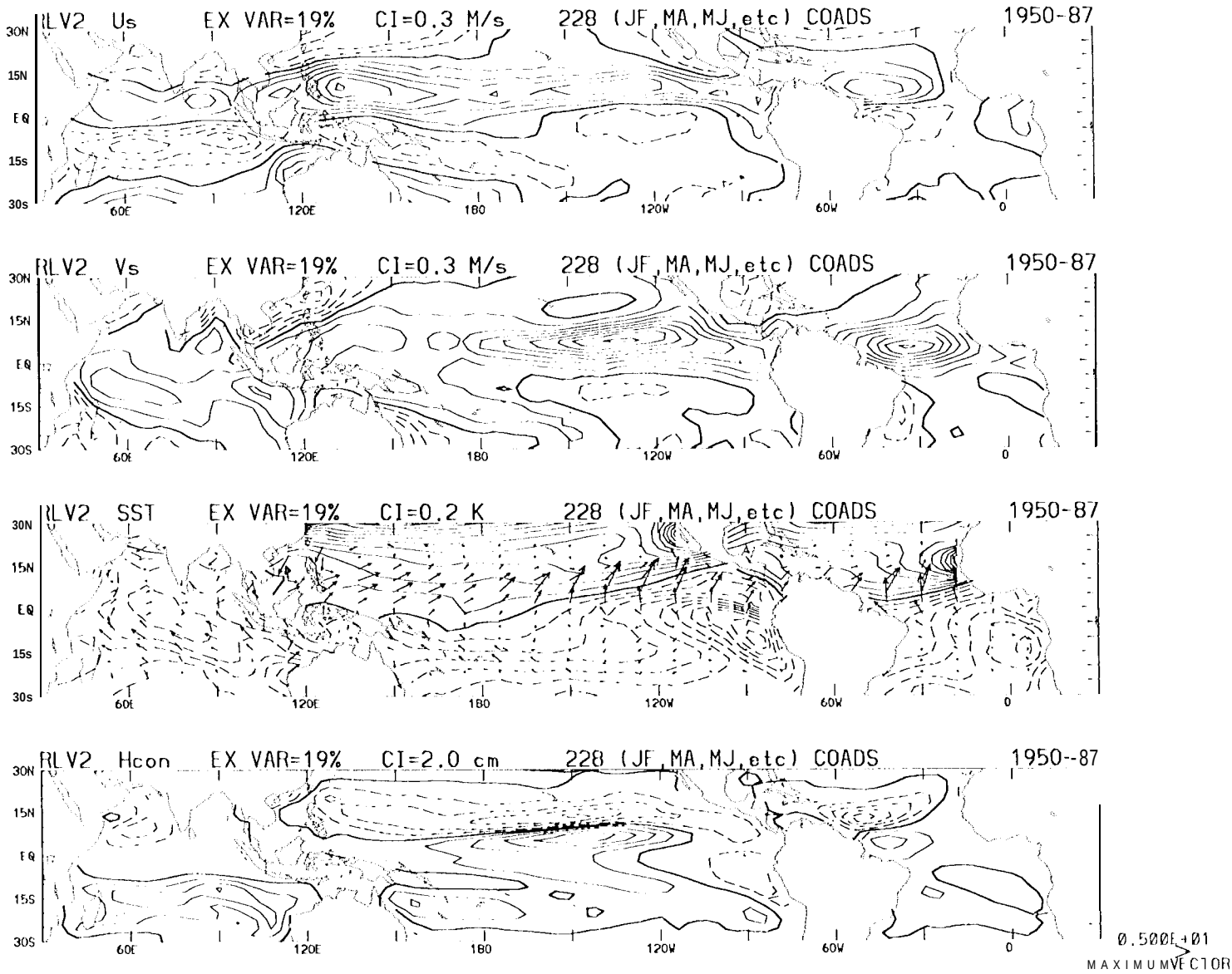

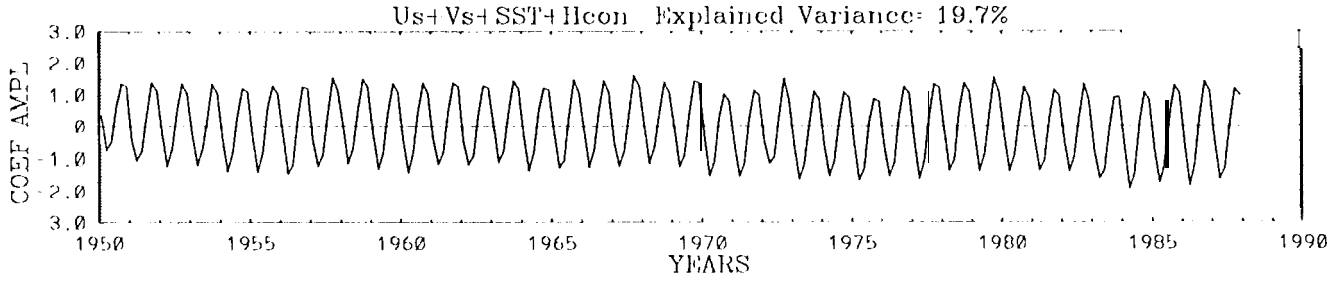

2. The second-leading mode of combined variability of two-month averaged COADS surface winds and SSTs, and simulated H_{con} anomalies. It represents extreme phases of annual-cycle related variability in the eastern ocean basins, and explains about 19% of the combined domain-averaged variance. Rest as in Fig. 1.

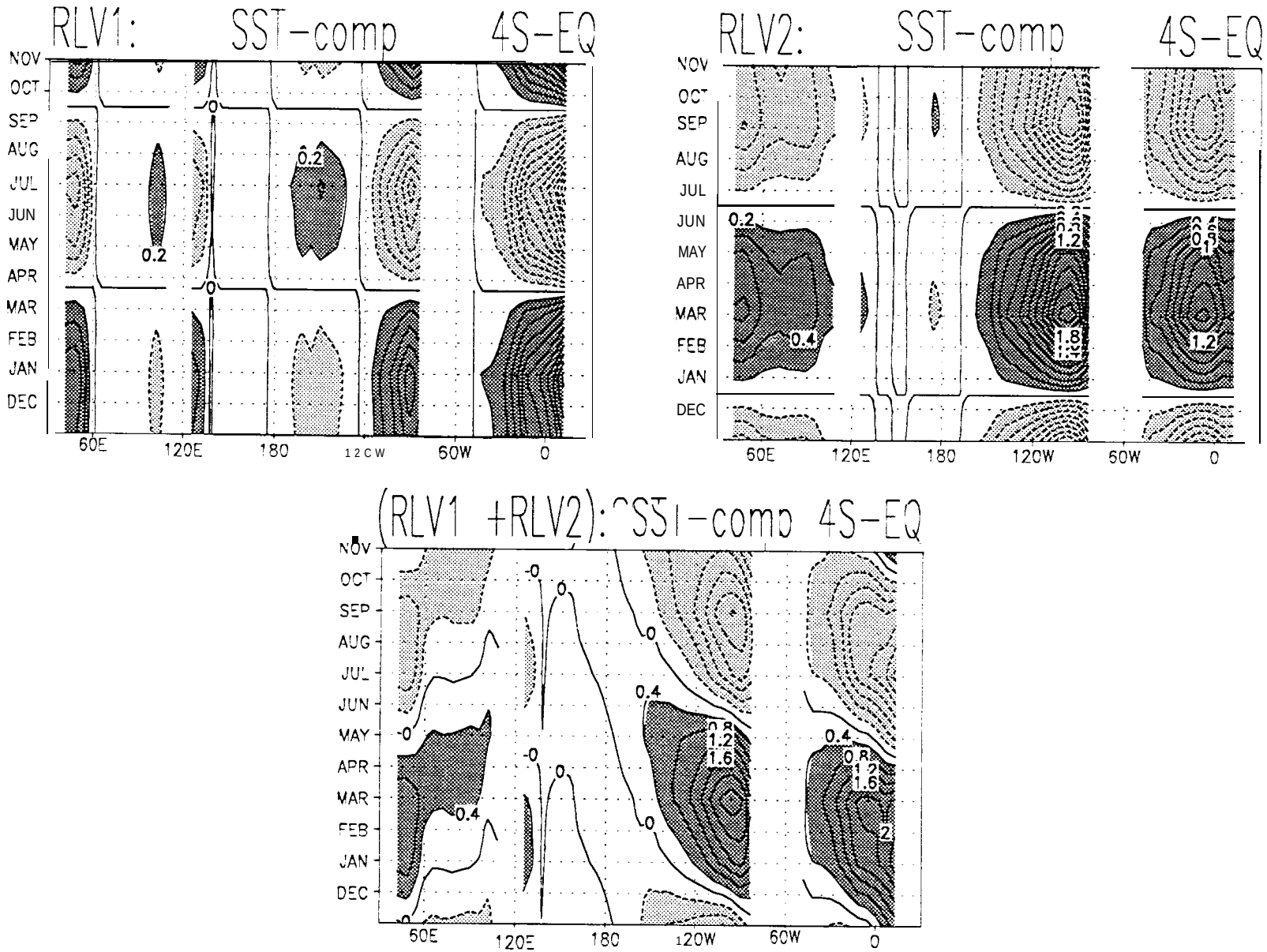

3. The temporal evolution of the 4°S–EQ band-averaged SSTS in the two-leading annual-cycle related variability modes (top-two panels), and in their sum (bottom panel). These displays arc obtained by multiplying the composite coefficient time-series (principal components) of each mode with the corresponding rotated loading vector. The contour interval and shading thresholds are 0.2°K in the top-two panels, and 0.4°K in the bottom panel. The month-markings are at the end of calendar months.

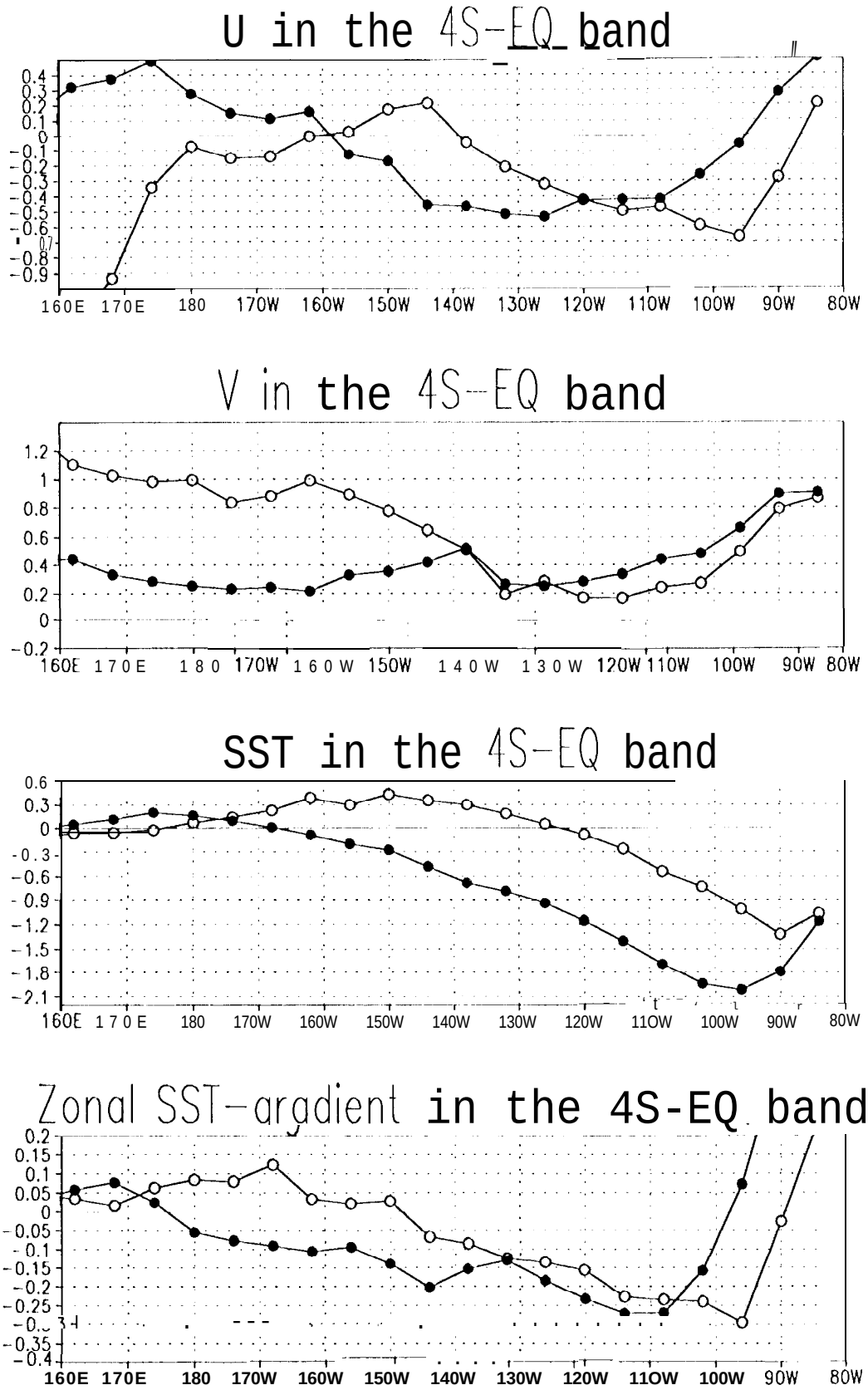

4. The longitudinal structure of July (open circles) and October (solid circles) annual-cycle related and '4°S-EQband-averaged' surface winds (top-two panels), SSTs (third panel), and zonal SS~"-gradients (bottom panel) to facilitate understanding of the zonal-momentum balance in the Pacific cold-tongue's core region.

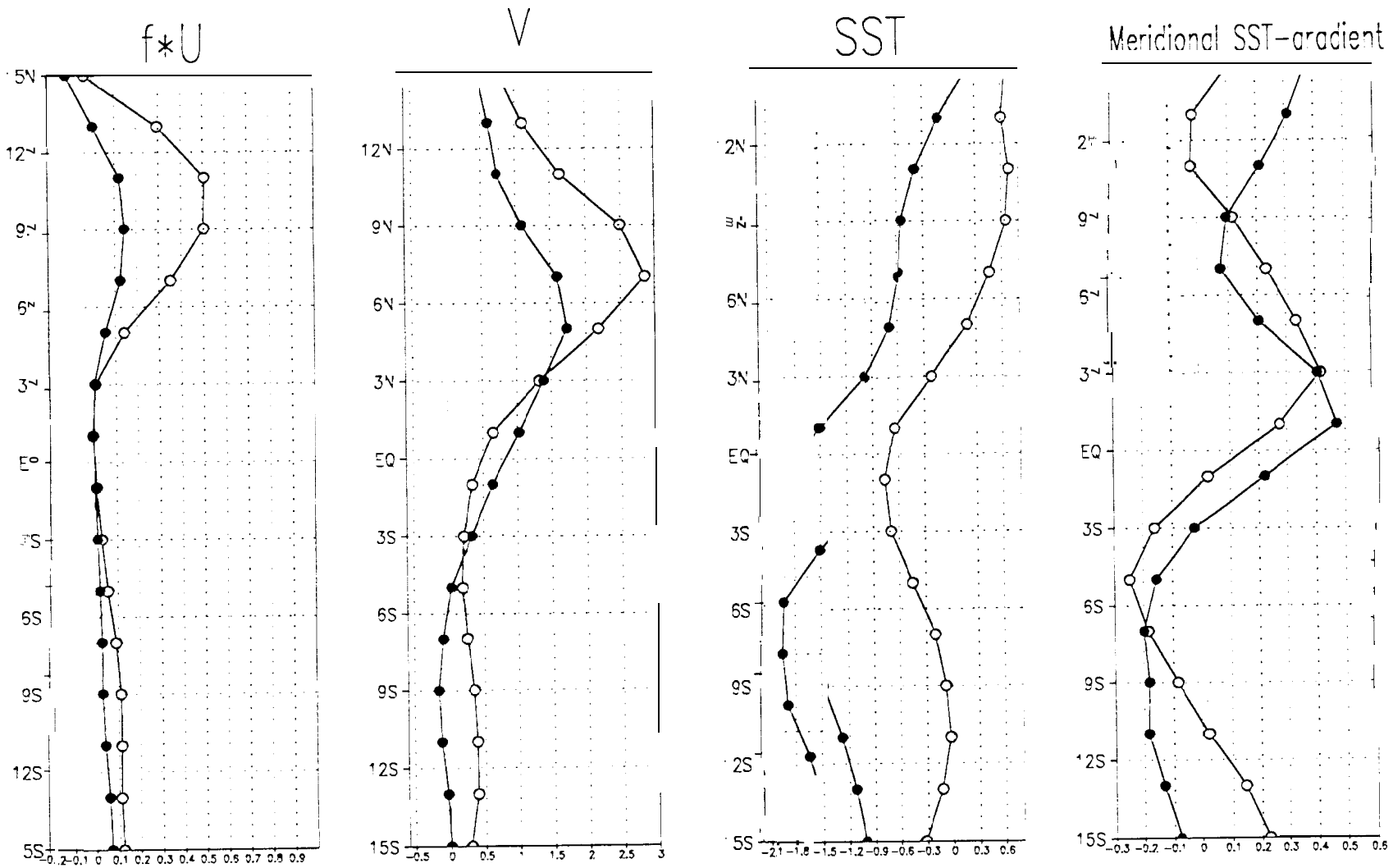

5. The latitudinal structure of July (open circles) and October (solid circles) annual-cycle related Coriolis force (f*u) and meridional surface-winds (left-two panels), SSTs (third panel), and meridional SST-gradients (right-most panel) to facilitate understanding of the meridional-momentum balance at a representative Pacific cold-tongue longitude (100°W).

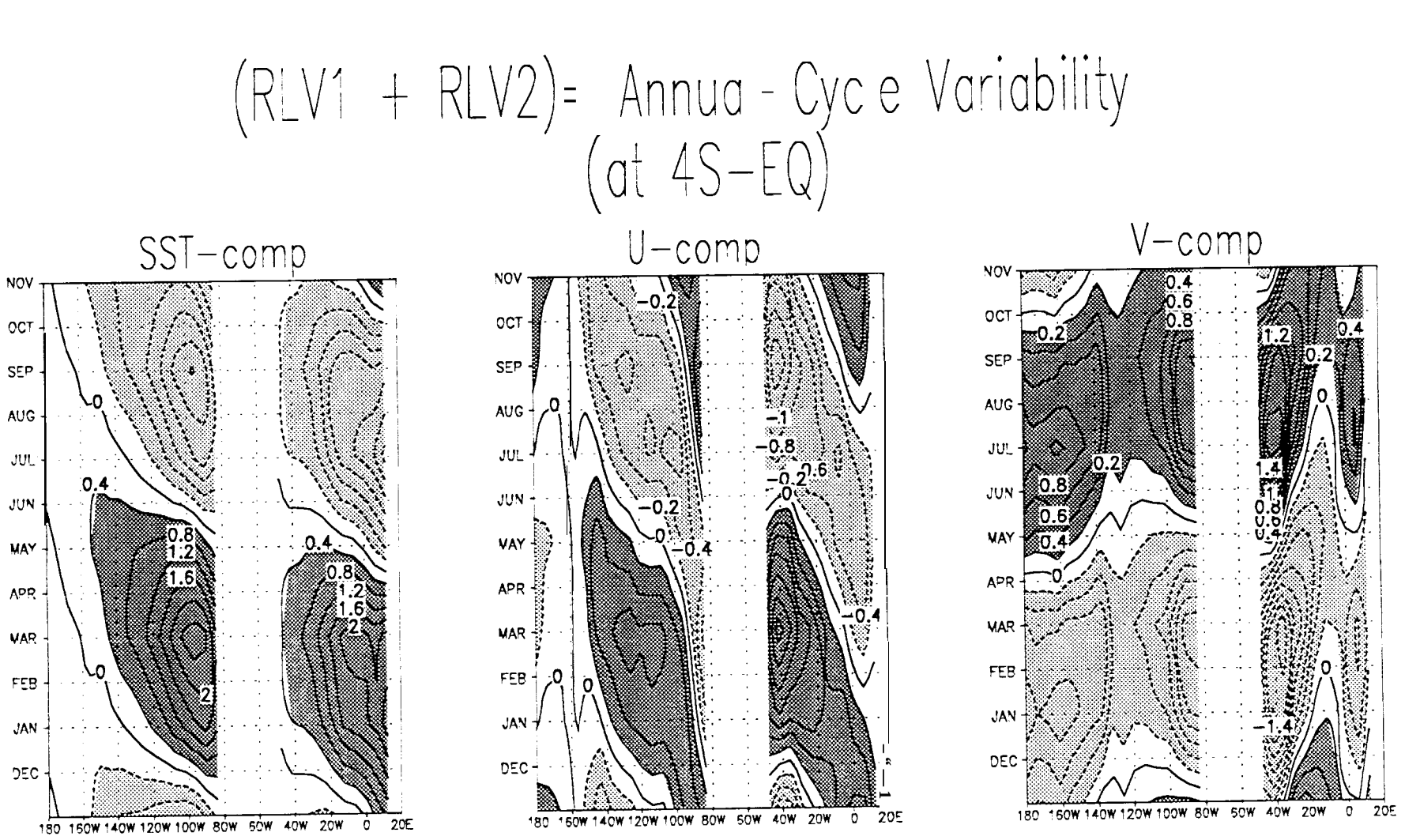

6. The temporal evolution of extracted total annual-cycle variability (: RLV1+RLV2) of the 4°S–EQ band-averaged SSTs and surface-winds in the eastern Pacific and Atlantic longitudes. The undertaken compositing is as described in the Fig. 3 caption. The contour interval and shading thresholds are 0.4°K in the SST-display, and 0.2 m/s in the surface-wind displays.

COADS Climatological Monthly-means based Annual Variability (at 4S-EQ)

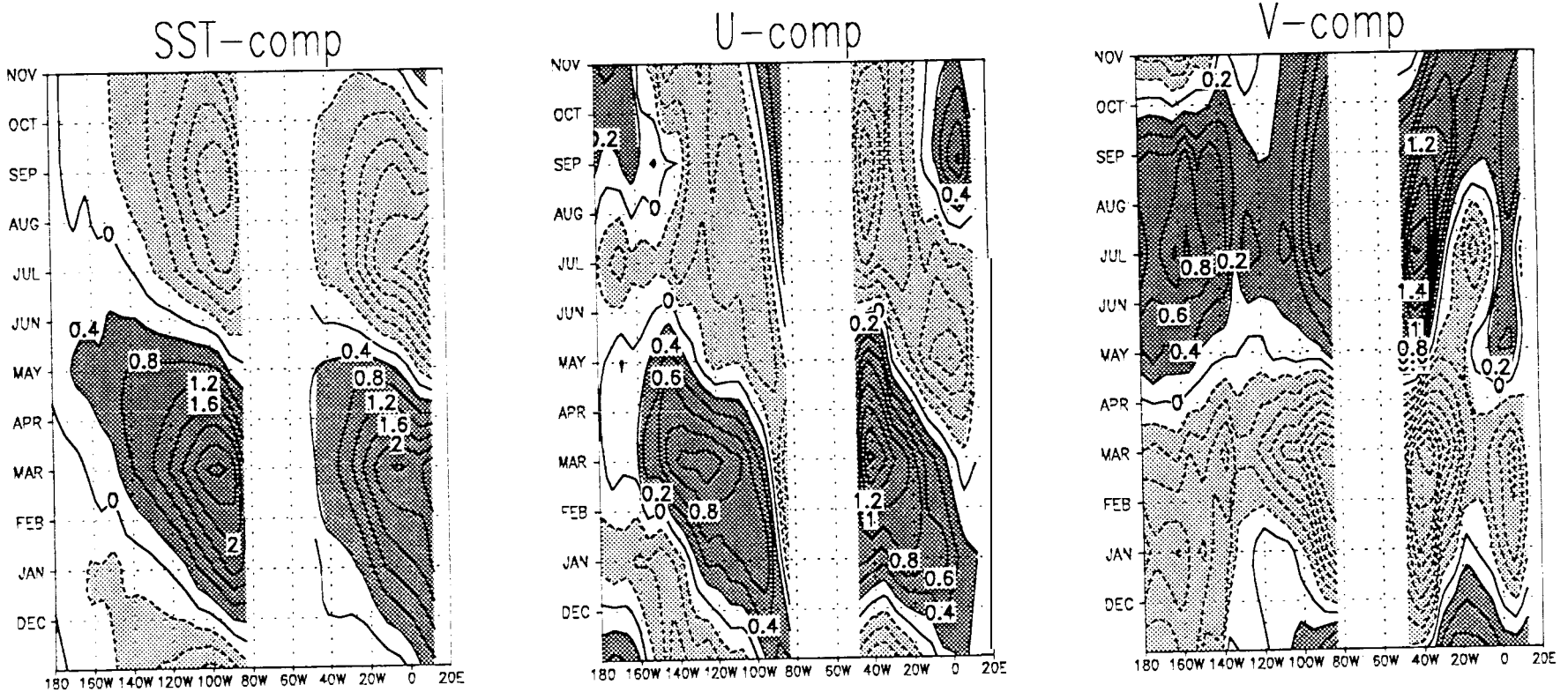

7. The temporal evolution of annual variability of COADS SSTs and surface-winds, calculated from the departures of climatological two-month averages from their climatological annual-means. Rest as in Fig. 6.

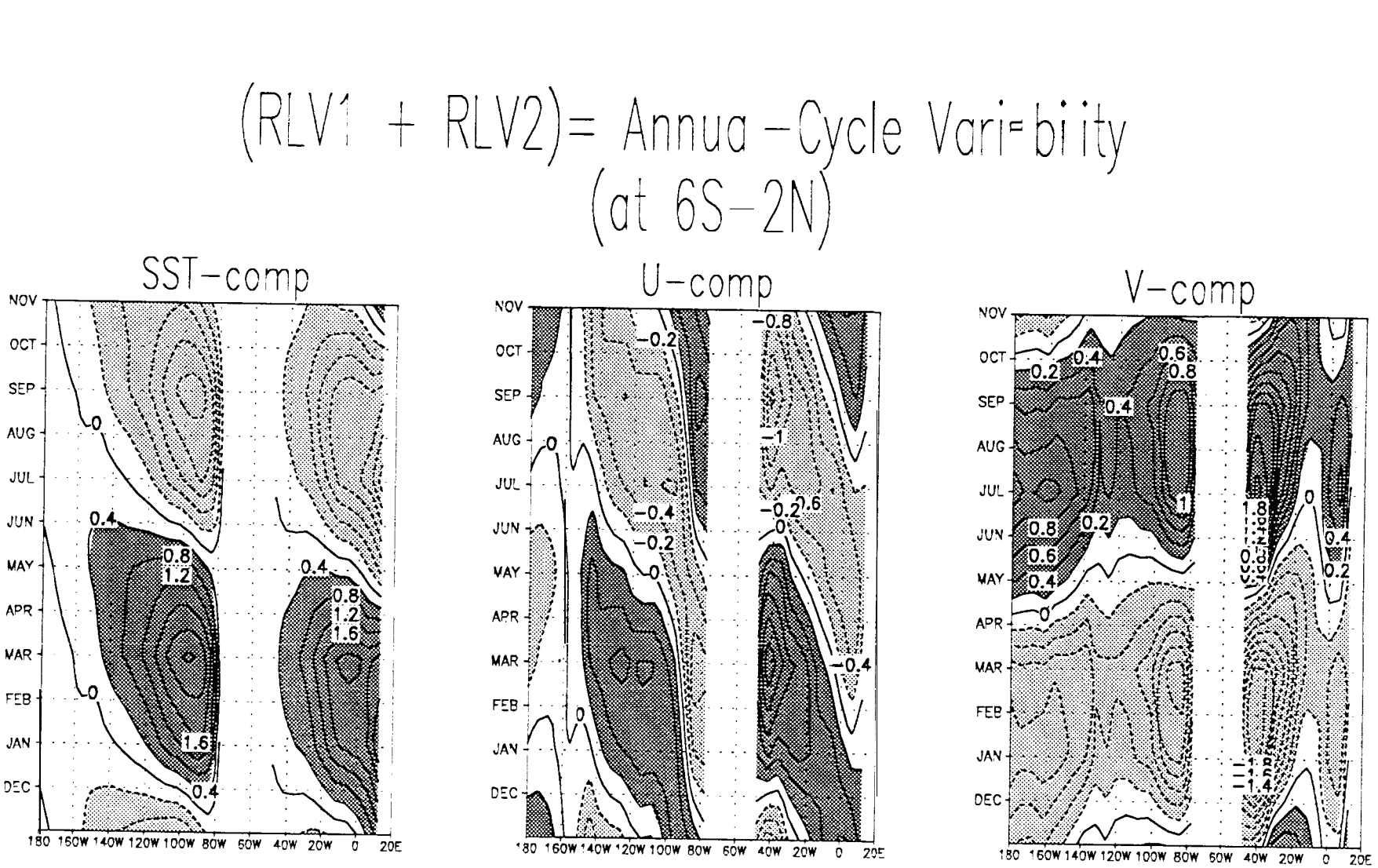

8. As in Fig. 6, but for the 6°S–2°N band-averages.

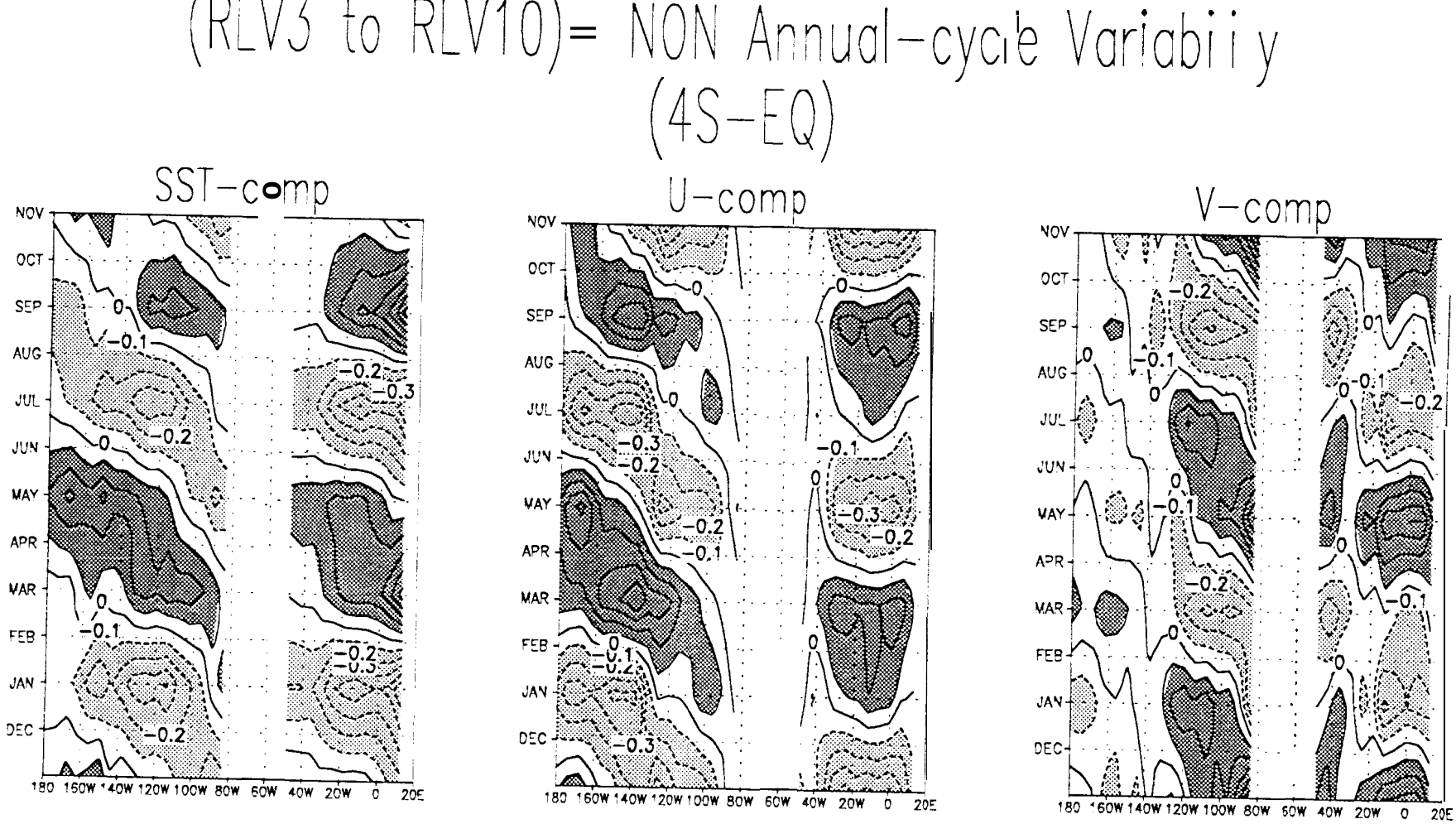

9. The temporal evolution of the extracted '*non* annual-cycle' variability (: sum of RLV3 to RLV10) of the 4°S–EQ band-averaged SSTs and surface-winds in the eastern Pacific and Atlantic longitudes. The undertaken compositing is as described in the Fig. 3 caption. The contour interval and shading thresholds are 0.1°K in the SST-display, and 0.1 m/s in the surface-wind displays.

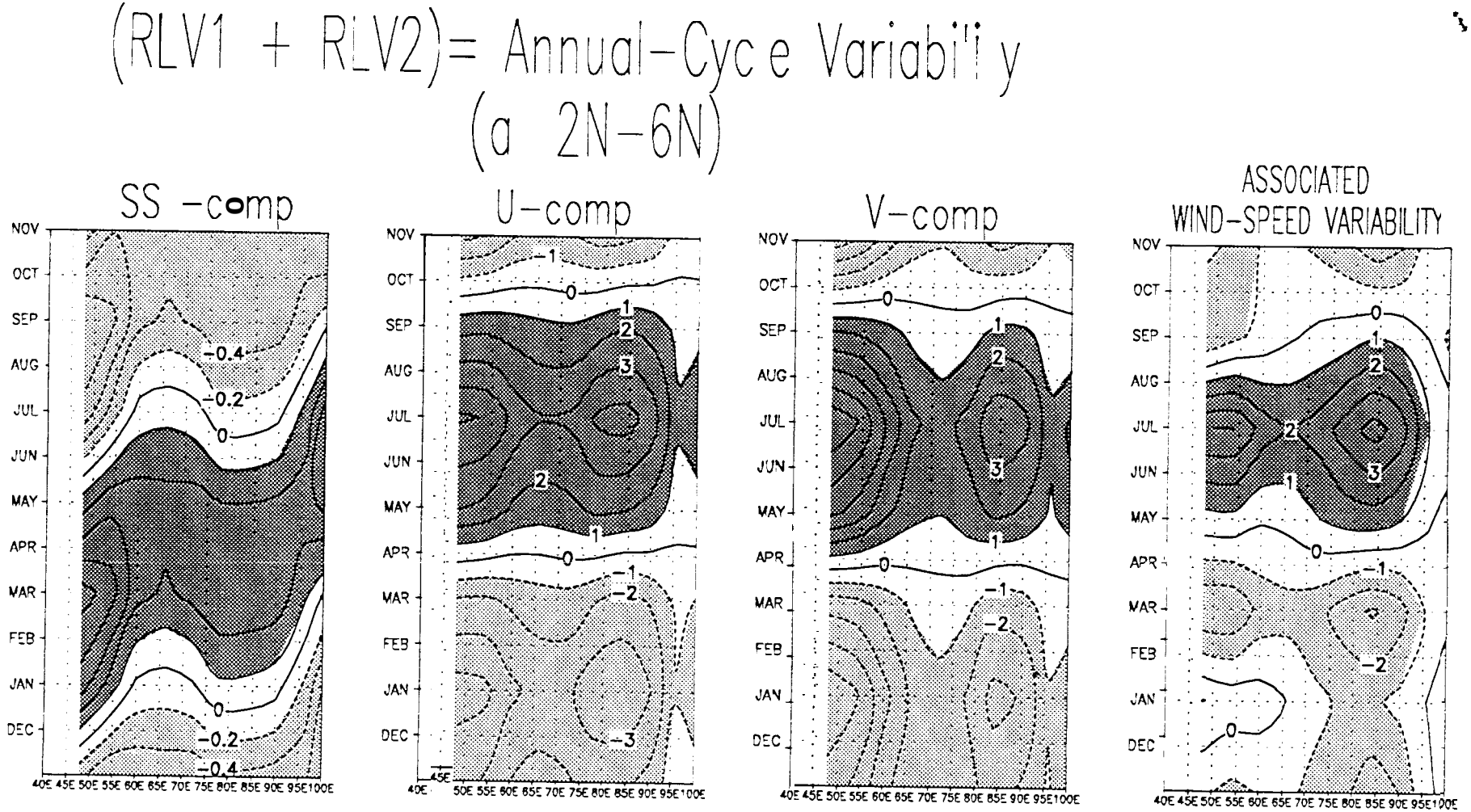

10. The temporal evolution of extracted total annual-cycle variability (: RLV1+RLV2) of the 2°N–6°N band-averaged SSTs and surface-winds in the Indian Ocean longitudes. The undertaken compositing is as described in the Fig. 3 caption. The right-most panel displays the evolution of associated surface wind-speed variability (see footnote 13 for more details). The contour interval and shading thresholds are 0.2°K in the SST-display, and 1.0 m/s in the other displays.